Research Article

Computational, Kinetics, and Corrosion Protection Aspects of Electrodeposited Poly(Salicylic Acid) Coatings as a Corrosion Inhibitor for Mild Steel

Ghada M. Abd El-Hafeez,[1] **Mohamed M. El-Rabeie** ®,[1] **El Hassane Anouar** ®,[2]
Moustapha E. Moustapha ®,[2] **Amany M. A. Osman** ®,[2,3] **and Zeinab R. Farag** ®[1]

[1]*Faculty of Science, Chemistry Department, Fayoum University, Fayoum 63514, Egypt*
[2]*Department of Chemistry, College of Science and Humanities in Al-Kharj, Prince Sattam Bin Abdulaziz University,
 Al-Kharj 11942, Saudi Arabia*
[3]*Chemistry Department, Faculty of Science, Menofia University, Shebin El-Koam, Menofia, Egypt*

Correspondence should be addressed to Zeinab R. Farag; zrf00@fayoum.edu.eg

Poly(salicylic acid) PSA has been electrochemically deposited onto a Pt electrode. The kinetics of the polymerization reaction has been studied. The polymer structure was confirmed and characterized using IR spectroscopy, XRD, SEM, and TGA analysis. The deposited PSA was then collected from the Pt surface and tested as a corrosion inhibitor for a mild steel electrode in an aqueous medium of 1 M sulfuric acid. The corrosion behavior was then evaluated using potentiodynamic polarization and electrochemical impedance spectroscopy (EIS). Corrosion measurements showed that the inhibition efficiency of 20, 50, and 100 ppm of PSA was 33, 57, and 74%, respectively. The inhibition mechanism was proved using adsorption isotherms as well as quantum calculations. The inhibition of the corrosion process was due to the adsorption of PSA on the steel surface, which was found to comply with the Langmuir adsorption isotherm.

1. Introduction

Mild steel is one of the main construction materials, which is extensively utilized in many industrial applications and devices. Its tendency to undergo indentation and corrosion in aqueous solutions especially in acidic medium is the major disadvantage despite its low cost and excellent mechanistic characteristics [1–3]. The acidic medium H_2SO_4 or HCl is used in manufacturing processes such as cleaning, pickling, and descaling as well as in oil drilling [4].

One of the main technological effective methods of corrosion protection used to reduce the rate of dissolution of metals is by applying inhibitors, which are mostly organic compounds carrying delocalized π-electrons and containing N, O, and/or S as hetero-atoms [5]. Conducting polymeric inhibitors CP have also been used due to their industrial applications and economic viability; upon adsorption of these polymers, they are able to block large areas of the corroding metal surface. On the other hand, polymers act as excellent inhibitors when used at low concentrations as compared to simple organic materials. The efficiency of these inhibitors depends on their ability to be adsorbed on the metal surface. A higher inhibition efficiency requires a higher molecular weight and a large molecular size of the inhibitor in order to ensure a greater coverage of the metallic surface [6].

Polyaniline derivatives (PANI), poly (diphenylamine), poly(aminoquinones) [1, 7–11], and phenylenediamine polymers have been investigated because of their inhibition features [12, 13]. The polythiophene (PTh), polypyrrole (PPy), and polycarbazole (PCz) have also been used as corrosion inhibitors [14–16]. Abd El-Hafeez et al. recently

used poly (salicylic acid-co-N-methylaniline), poly(SA-co-NMA), and poly(o-bromophenol-co-N-methylaniline), (poly(OBP-co-NMA)) as corrosion inhibitors for mild steel [17, 18]. The results showed that the used polymers increased the corrosion protection efficiency of the passivated mild steel samples. Hydrazide derivatives were also used and showed a good inhibition effect [19, 20].

Phenols and polyphenols were also investigated as corrosion inhibitors [21–23]. Aljeaban et al. recently studied decorated polymers with functional motifs for the mitigation of steel corrosion [24]. The diverse structures of phenol polymers lend them various biological and chemical applications such as antioxidant activity, antibiotic, and antifouling actions. Veys-Renaux et al. studied the morphological, structural, and electrochemical effects of some polyphenolic compounds, mainly esculetol, esculin, and rutin on the corrosion behavior of steel in a weak acidic medium containing 10^{-3} M NaCl at pH = 4 [22]. The inhibitory effect of polyphenols extracted from *Artemisia herba-alba* (AHA) on mild steel corrosion in a 1 M HCl solution was tested, and the results showed that the effectiveness of inhibition was 92.9% at 900 ppm [25]. The preventive effect of some phenol Schiff bases on the corrosion of mild steel in acidic medium revealed that the protective efficacy for the used inhibitors improves with decreasing temperature and rises with concentration [26]. The effect of tannins as corrosion inhibitors of bare and coated aluminum alloys 1200 was investigated by Nardeli et al. [27].

The effect of using green inhibitors, namely, *Rosmarinus officinalis RO* polyphenols, on the corrosion behavior of XC48 steel in an acidic medium has been studied. Results show that the *RO* behaved as a mixed inhibitor and the inhibition efficiency increased with increasing the concentration of the inhibitor and decreased with the rise of the temperature [28]. Another phenolic ecofriendly extract of *Ammi visnaga* was also examined as a corrosion inhibitor for mild steel in acidic medium. Potentiodynamic and electrochemical impedance spectroscopy (EIS) studies showed that the tested species act as mixed-type corrosion inhibitors [29].

Chung et al. studied the corrosion behavior of mild steel in 1 M H_2SO_4 containing *Cucumis anguria* L. (*C. anguria* L.) as a corrosion inhibitor [30]. The maximum inhibition efficiency was found to be 92.39% for 250 ppm of the *C. anguria* L. leaf extract inhibitor. The synergistic effects of cerium nitrate on the corrosion retardation ability of the tannic acid (TAA) were tested in a NaCl solution [31].

The corrosion behavior of mild steel was studied in the presence of some commercial inhibitors in phosphoric acid, the higher inhibition efficiency was 31.60% at a 0.2 mL/L concentration of Corrogard [32]. The inhibitive impact of the ecofriendly polyester (Glyptal) was also examined, and it showed an inhibition efficiency of 67.32 and 90.72% at 100 and 1000 ppm, respectively [33]. Gravimetric techniques were used to test some thiazole derivatives, namely, APNT and APT, as organic inhibitors in 1 M HCl solution, the inhibition efficiency of APNT decreases from 97.1 to 80.4% in the temperature range 303 K to 333 K and decreases sharply from 94.1 to 52.6% for APT [34]. The inhibition action of some amine compounds on the corrosion of mild steel in HCl was studied; 0.1 M of anthranilic acid, o-phenylenediamine, and p-toluidine gave inhibition efficiency of 85.11, 38.71, and 29.63%, respectively [35]. Some organic acids were investigated as inhibitors for mild steel. Benzoic acid and salicylic acid were investigated in a sulfuric acid medium. The inhibition efficiency of 0.001 M of the used acids at 313 K was 41% for benzoic acid and 47% for salicylic acid [36]. Anthranilic acid was tested in 1°M HCl and the inhibition efficiency was 64.6% at 500 ppm and 303 K [37]. Ade studied the inhibition efficiency of 20 mg of benzoic acid, salicylic acid, anthranilic acid, 2-nitro benzoic acid, and 2-chloro benzoic acid in different acidic media. The higher inhibition efficiency was 32.43% for anthranilic acid in 0.1 N H_2SO_4, 66.66% for 2-chloro benzoic acid in 0.01 N H_2SO_4, and 80.95% for anthranilic acid in 0.001 N H_2SO_4 [38].

SA was tested as a corrosion inhibitor and it showed good inhibition efficiency; the aim of choosing PSA is the higher m.wt of the polymer, which will allow an excellent surface coverage compared to SA, and the functionality increases also which increases the active sites to be absorbed to the metal surface.

In this work, an extensive kinetic study for the electropolymerization of salicylic acid was accomplished. The deposited poly (salicylic acid), PSA, was collected from the Pt-electrode surface, characterized, and then, it was examined as a corrosion inhibitor for mild steel in 1 M H_2SO_4.

2. Materials and Experimental Procedures

2.1. Materials and Solutions. Salicylic acid was obtained from (Merck Schuchardt, Germany), and sulfuric acid, ethanol, and acetone were provided by El Nasr Company for Intermediate Chemicals (Egypt). The used chemicals were of analytical grade and were used as received. All solutions were prepared using fresh deionized water.

2.2. Electrochemical Measurements. A three-electrode system was applied to evaluate the electrochemical performance of the mild steel electrode in a naturally aerated stagnant 1 M H_2SO_4 solution (pH = 2). A VoltaLab potentiostat (Radiometer PGZ301) was utilized for all electrochemical measurements. A saturated calomel electrode SCE and a Pt-electrode were used as the reference and counter electrodes, respectively.

The Pt electrode was a Pt foil with dimensions of 1 cm length and 0.5 cm width containing a platinum wire (0.75 cm) to facilitate the electrical connection, and it was cleaned and dried before each measurement.

The working electrode was a mild steel rod of 0.5 cm^2 surface area, and its chemical composition is listed in Table 1. The mild steel electrode was polished by consecutive emery papers ranking from 600–2500 grit; then, it was washed and dried using a soft paper. EIS was performed at a steady state potential, and it was performed within the frequency range of 100 000–0.1 Hz with a peak-to-peak amplitude of 10 mV [39, 40]. The electrochemical impedance

parameters have been fitted using the Z_m view software with a suitable equivalent circuit [17, 41].

Potentiodynamic polarization measurements were executed over the sweeping potential range of −1200 to −100 mV at a scan rate of 10 mVs^{-1}. Subsequently, the steel electrode was directly dipped in the corrosive medium. To verify the reproducibility, every experiment was repeated at least three times.

2.3. Preparation of Poly (Salicylic Acid).

The electropolymerization of SA at concentrations ranging from 0.01 to 0.05 mol·L^{-1} in an aqueous solution of 0.2 mol·L^{-1} H$_2$SO$_4$ was performed at 313 K with the desired scan rate.

To obtain the required concentration of the polymer, a certain amount of it was dissolved in 1 M H$_2$SO$_4$ solution. Then, a series of solutions with lower concentrations were prepared by dilution.

2.4. Determination of the Reaction Rate of Electropolymerization.

The reaction rate of the electropolymerization reaction was determined using the following equation:

$$\text{Rate} = k[\text{Monomer}]^a \left[\text{H}_2\text{SO}_4\right]^b, \tag{1}$$

where k is the rate constant of the electropolymerization reaction.

The apparent activation energy E_a was calculated using the following equations:

$$\frac{d\ln k}{dt} = \frac{E_a}{RT^2}, \tag{2}$$

where (k) is the rate constant, (T) is the absolute temperature, and (R) is the universal gas constant. By integration, we obtain as follors:

$$\ln k = \frac{-E_a}{RT} + C,$$
$$\text{Log} k = \frac{-E_a}{2.303R\,(1/T)} + C', \tag{3}$$

where C and C' are constants.

To check the validity of the Arrhenius equation, a plot of log k against $1/T$ should give a straight line with a slope of $(-E_a/2.303\ \text{R})$. In the present work, the value of k was substituted by the values of the initial rates of the electropolymerization, and by plotting the values of the log rate against $1/T$, a straight line was obtained. The apparent activation energy (E_a) was calculated from the slope of the straight line.

Enthalpy of activation (ΔH^*) and entropy (ΔS^*) were calculated using the activated state theory equation (Eyring equation):

$$K = \frac{RT}{Nh} e^{(\Delta S^*/R)} e^{(-\Delta H^*/RT)} \text{ or } \frac{K}{T} = \frac{k}{h} e^{(\Delta S^*/R)} e^{(-\Delta H^*/RT)}, \tag{4}$$

where K is the Boltzmann constant, h is Plank's constant, R is the universal gas constant, and T is absolute temperature. Taking the natural logarithmic:

$$\text{Log}\left(\frac{K}{T}\right) = \text{Log}\left(\frac{k}{h}\right) + \left(\frac{\Delta S^*}{2.303\text{R}}\right) - \left(\frac{\Delta H^*}{2.303\text{R}}\right)\left(\frac{1}{T}\right). \tag{5}$$

The plot of Log (K/T) against $1/T$ gives a straight line with a slope that equals to $(-\Delta H^*/2.303\ \text{R})$ and an intercept that equals to $(\text{Log }(k/h) + (\Delta S^*/2.303R)$. Therefore, the enthalpy of activation (ΔH^*) and entropy (ΔS^*) can be calculated from the slope and intercept of the abovementioned relationship, respectively.

2.5. Characterization of the Electrodeposited Polymer

(i) Ultraviolet spectroscopy was carried out using a Shimadzu UV spectrophotometer (M160 PC) at room temperature in the range from 200–400 nm using ethyl alcohol as the solvent and reference.

(ii) Infrared measurements were carried out using a Shimadzu FTIR-340 Jasco spectrophotometer (Japan) using KBr pellets on a disk.

(iii) ^{1}HNMR measurements were performed with a Varian EM 360 L, 60 MHz NMR spectrometer. Dimethylsulphoxide (DMSO) was used as the solvent.

(iv) Thermogravimetric analysis (TGA) was performed using a Shimadzu DT-30 thermal analyzer (Shimadzu, Kyoto, Japan). The measurements were recorded from RT up to 600°C (20°C/min) under N$_2$ with a flow rate of 50 mL/min.

(v) Scanning electron microscopy (SEM) was carried out on a PSA film deposited onto the Pt surface using a JSM-T20 Electron Probe Microanalyzer (JEOL, Tokyo, Japan). The X-ray diffraction analysis (XRD) (Philips 1976 Model 1390, the Netherlands) was operated using a Cu X-ray tube, scan speed: 8 deg/min, current: 30 mA, voltage: 40 kV, and preset time: 10 sec.

2.6. Quantum Calculations.

In addition to experimental measurements, the corrosion efficiency of salicylic acid (SA) and its polymer (PSA for $n = 2$) was investigated using DFT calculations and molecular mechanics. First, the stable conformers of SA and PSA were optimized using the hybrid functional B3LYP and the basis set 6-31G (d) as implemented in Gaussian 16 W software [42]. The optimization was followed by frequency calculations, which confirmed that the ground states of optimized geometries SA and its dimer were true minima. To correlate the corrosion inhibition of SA and its dimer to their molecular and electronic properties, a set of these properties were calculated. Among the properties calculated are ionization potential (IP), electronic affinity (EA), gap energy between the HOMO and LUMO (ΔE), electronegativity (χ), chemical hardness (η), softness $(S = 1/\eta)$, electrophilicity (ω), and dipole moment (μ) using the following formulae:

TABLE 1: The chemical composition (weight %) of the mild steel electrode.

Element	C	Si	Mn	S	P	Cu	Cr	Ni	Al	Fe
Analysis	0.34	0.26	0.93	0.02	0.04	0.01	0.01	0.02	0.01	Balance

$$IP = -E_{HOMO},$$

$$EA = -E_{LUMO},$$

$$\chi = \frac{IP + EA}{2},$$

$$\eta = \frac{(IP - EA)}{2},$$

$$S = \frac{1}{\eta}, \tag{6}$$

$$\omega = \frac{\mu^2}{2\eta},$$

$$\mu = \sqrt{\mu'^2_x + \mu'^2_y + \mu'^2_z}.$$

In addition, the fraction of the transferred electrons (ΔN) between the inhibitors SA and PSA from one side and the metal/solution interface was calculated using the Pearson theory [43] as shown in the following equation:

$$\Delta N = \frac{\chi_{Fe} - \chi_{inh}}{2(\eta_{Fe} + \eta_{inh})}, \tag{7}$$

where χ represents the electronegativity, Fe denotes the iron atom, η indicates the hardness, and inh stands for SA and PSA inhibitors. Moreover, the corrosion inhibition efficiency of SA and its dimer may depend on the nucleophilic and electrophilic sites that may bind/interact with the metal/solution interface. The electrostatic potential (ESP) and frontier molecular orbital (FMO) of SA and PSA were determined at the same level of theory. In ESP maps, the red color indicates the negative region, which corresponds to hydrogen bond acceptors; while the blue color is an indication of the positive region, which corresponds to hydrogen bond donors. The solvation effects were taken into account implicitly by using the integral equation formalism variant polarizable continuum model (IEFPCM) and water as the solvent. In this model, the inhibitor is embedded in a cavity surrounded by a solvent described by its dielectric constant ε (e.g., for water $\varepsilon = 78.3553$) [44]. Gauss View 6 is used for visualization of the ESPs, frontier molecular orbitals HOMO and LUMO. Molecular mechanics calculations were carried out using the COMPASS force field in the Forcite model as implemented in the Material Studio package (BIOVIA Accelrys, San Diego, CA, USA, 2014). The adsorption energies of SA and its dimer on the metal surface was calculated using the following formula:

$$E_{ad} = E_{Inh-Fe} - (E_{Fe} + E_{Inh}), \tag{8}$$

where Inh denotes the inhibitor.

3. Results and Discussion

3.1. Electropolymerization of Poly (Salicylic Acid). Cyclic voltammetry of SA in 0.30 mol·L^{-1} H_2SO_4 with a scan rate of 40 mVs^{-1} at 313 K. The cyclic voltammogram started from -500 to $+2000 \text{ mV}$ (vs. SCE), as shown in Figures 1(a) and 1(b). In the absence of SA, an oxidation peak developed at -260 mV due to adsorption of hydrogen on the Pt electrode [45] (Figure 1(a)). On the other side, in the presence of 0.04 mol·L^{-1} SA, two oxidation peaks (I and II) appeared at -260 and $+1170 \text{ mV}$, respectively, while the oxidation peak (II) decreases with the formation of PSA and a reduction peak (II$'$) was developed at $+220 \text{ mV}$ (Figure 1(b)). The first oxidation peak (I) is a result of hydrogen reduction [45] while the second oxidation peak (II) corresponds to a phenoxy-radical, which was adsorbed on the Pt electrode as a result of the oxidation of the monomer [46]. The adsorbed radicals react via head-to-tail coupling with other SA molecules to form a para-linked dimeric radical forming polymeric film. This film is a chain of isolated aromatic rings (polyethers) without π-electrons delocalization between each unit as shown later in Scheme 1.

The oxidation occurred at more positive values ($+1170 \text{ mV}$) as the oxidation process became difficult due to the presence of a carboxyl group (COOH). The reversing anodic current was very small indicating the formation of a good adhered polymer layer on the Pt surface [47]. The cathodic peak (II$'$) which could be ascribed to the reduction of the electrodeposited polymer film (quinoidal structure) [47]. However, once polymerization was started, a brown polymer film was rapidly deposited on the surface of the Pt electrode. The potential difference between the two oxidation peaks (I and II) was about 1430 mV, and no additional peaks were observed between them, which confirmed the absence of degradation products and also indicate a higher homogeneity and regularity of the polymer film.

3.1.1. Effect of Repetitive Cycling. The effect of repetitive cycling on the polymerization reaction is represented in Figure 2. The peak currents (I_{pI}, I_{pII}, and $I_{pII'}$) decreased with increasing the cycling up to 7 cycles, which reveals the effect of H_2 reduction on the surface area of the electrode peak (I), while the oxidation peak (II) decreases significantly with repetitive cycling [45]. The formed polymeric film hinders the diffusion of further phenoxide ions to the electrode surface, causing a significant decrease in both the anodic and the cathodic peak currents. The redox reactions were independent of the polymer thickness; this was evident from the potential position of the redox peaks, which did not shifted with an increasing number of cycles [48]. The low anodic currents may be attributed to the presence of a polymer film on the electrode surface.
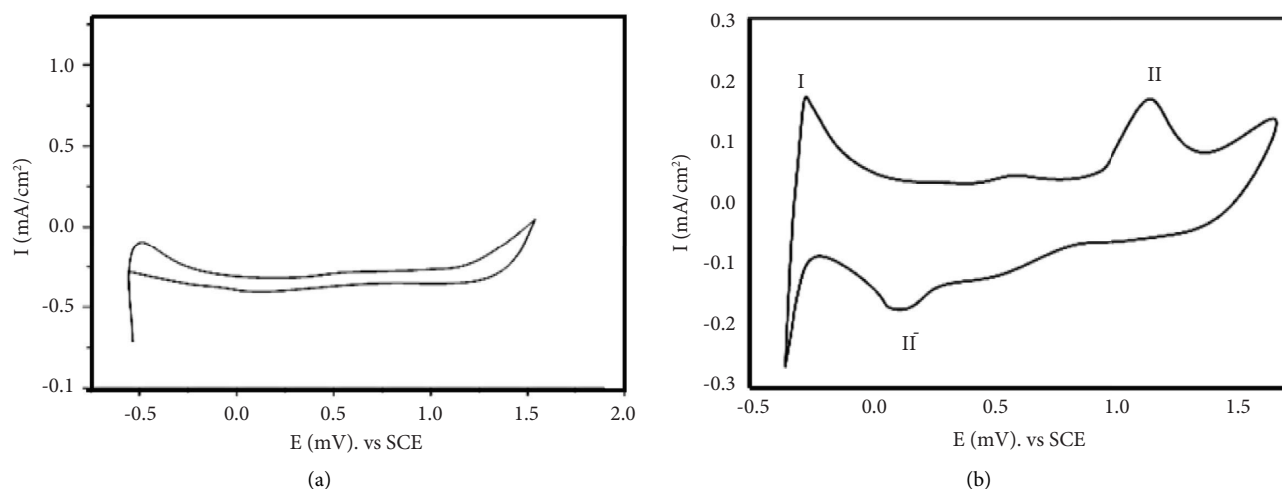
(a)

(b)

FIGURE 1: Cyclic voltammograms of a solution containing 0.30 mol·L^{-1} H$_2$SO$_4$ at 313 K with scan rate of 40 mVs^{-1}. (a) Without SA and (b) with 0.04 mol·L^{-1} SA.

3.1.2. Effect of the Scan Rate. The effect of the scan rate ranged from 25–40 mVs^{-1} on the potentiodynamic anodic polarization curves for the electropolymerization process as shown in Figure 3(a). The results showed that both anodic and cathodic peak current density (I_{pII} and $I_{pII'}$) increased with increasing the scan rate up to 40 mVs^{-1} and then decreased after a scan rate of 40 mVs^{-1}.

Figure 3(b) shows the linear dependency of the anodic peak current densities (I_{pII}), which corresponds to the formation of the PSA layer versus the square root of the scan rate ($v^{1/2}$). This linear relationship indicated that the oxidation of SA to PSA is a partially diffusion-controlled process, with the correlation coefficient (r^2) being higher than 0.9 ($\neq$1.0), indicating a non-ideal simulation relationship. Values of (I_{pII}) are directly proportional to ($v^{1/2}$) according to the Randles and Sevick equation [49]:

$$I_{pII} = 0.4463 \, n \, FAC \left(n \frac{FvD}{RT} \right)^{1/2}, \quad (9)$$

where n is the number of exchanged electrons, F is Faraday's constant (96485 C/mol), A is the electrode surface area (cm^2), C is the bulk concentration of the analyst diffusing coefficient (cm^2/s), v is the scan rate, R is the universal gas constant (8.314 Jmol^{-1} K^{-1}), and T is the absolute temperature (K). The calculated values of diffusion coefficients (D) at 0.30 mol·L^{-1} H$_2$SO$_4$ and 0.04 mol·L^{-1} SA at 313 K with different scan rate values ranging from 25–40 mVs^{-1} are shown in Table 2.

The formation of radical cations is controlled by the charge transfer process. When the polymers became thick, the diffusion of the reactant within the film became a slower step, and the process changed to diffusion transfer Figure 3(a). The intercept in Figure 3(b) is small, −0.155 for SA, as a result of reducing of the active area of the working electrode during positive scanning due to the increase of the area covered by the deposited polymer film [50].

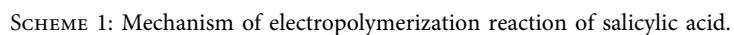*3.1.3. Kinetic Studies.* The kinetics of the electropolymerization reaction were investigated using an aqueous solution containing different monomer concentrations in the range between 0.01– and 0.04 mol·L^{-1} and H$_2$SO$_4$ concentrations in the range between 0.08– and 0.30 mol·L^{-1} at 313 K Figures 4 and 5, respectively. The cyclic voltammogram for each monomeric system was measured, and the relationship between the logI$_{pII}$ vs. log [SA] or logI$_{pII}$ vs. log [H$_2$SO$_4$] was plotted.

(1) Effect of SA Concentration. The effect of SA concentrations ranging from 0.01–0.05 mol·L^{-1} on the electropolymerization process is represented in Figure 4(a). The anodic peak current density (I_{pI} and I_{pII}) increased with increasing the monomer concentration up to 0.04 mol·L^{-1}. At higher concentrations (>0.04 mol·L^{-1}), no significant increase in peak currents was observed, indicating that the oxidation reaction at higher monomer concentrations is not limited by diffusion alone. The anodic peak current density (I_{pII}) was determined for different SA concentrations and is represented in Figure 4(a).

Figure 4(b) illustrates that the double logarithmic plot of the initial rates of electropolymerization reaction Log (Ri) versus the monomer concentrations created a straight line with a slope equal to 0.887, indicating that the order of the electropolymerization reaction was a first-order reaction.

(2) Effect of H$_2$ SO$_4$ Concentration. The effect of H$_2$SO$_4$ concentration (0.08–0.30 mol·L^{-1}) on the electropolymerization process is shown in Figure 5(a). The anodic peak current density (I_{pI} and I_{pII}) increased with the increase in H$_2$SO$_4$ concentration values up to 0.3 mol·L^{-1}. At higher concentrations (>0.30 mol·L^{-1}), no significant increase in peak currents was observed. This indicated that at higher concentrations, the oxidation reaction was not limited by diffusion alone.

Figure 5(b) illustrates that the double logarithmic plot of the initial rates of electropolymerization reaction Log (R_i) versus H$_2$SO$_4$ concentrations, which provided a straight line with a slope equal to 0.877, which suggested that the order of the electropolymerization reaction was a first-order reaction. The kinetic rate law can be written as follows:

1- Initiation

Scheme 1: Mechanism of electropolymerization reaction of salicylic acid.

$$R_p, E = k[\text{SA}]^{0.887}[\text{H}_2\text{SO}_4]^{0.887}, \tag{10}$$

where R_P and E represent the electropolymerization rate and k is the rate constant, respectively.

(3) Effect of Temperature and Calculation of Thermodynamic Parameters. Figure 6(a) represents the potentiodynamic polarization curves as a function of the solution temperature in the range between 298 and −313 K under the optimum
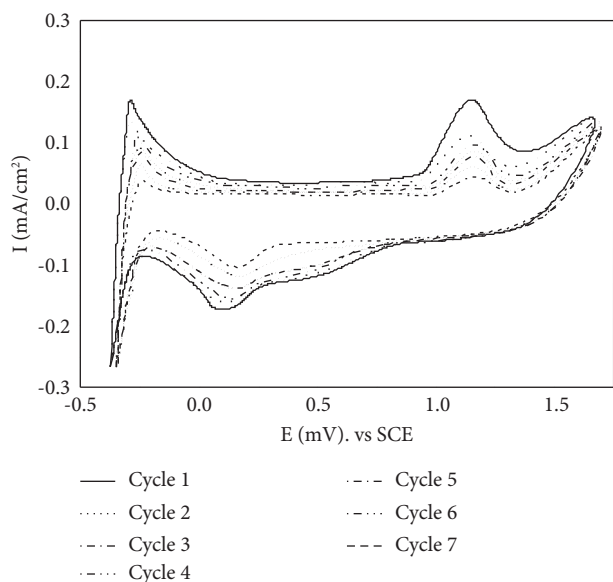
FIGURE 2: Effect of repetitive cycling on the cyclic voltammograms of the electropolymerization of SA from a solution containing $0.04 \, \text{mol·L}^{-1}$ SA and $0.30 \, \text{mol·L}^{-1}$ H_2SO_4 at 313 K with a scan rate of $40 \, \text{mVs}^{-1}$.

experimental conditions ($0.04 \, \text{mol·L}^{-1}$ SA and $0.3 \, \text{mol·L}^{-1}$ H_2SO_4). The anodic peak (II) increased with increasing temperature up to 313 K but above 313 K, the anodic peak (II) decreased.

Generally, the rate of the electropolymerization reaction is accelerated by raising the temperature. The variation of the rate constant with the temperature follows the Arrhenius equation:

$$\text{Rate constant} \, (k) = Ae^{-E_a/RT}. \tag{11}$$

An alternative form was obtained by taking the logarithm of each side. The initial rate (R_i) of the electropolymerization reaction was calculated at different temperatures ranging from 298 to 313 K; the data are represented in Figure 6(a).

The apparent activation energy (E_a) was calculated by plotting the logarithm of the initial rate log (I_{pI}) versus $1/T$ (Figure 6(b)), which gives a straight line with a slope equal to -2.8298. By applying the Arrhenius equation [47], the apparent activation energy was calculated and found to be $54.18 \, \text{kJmol}^{-1}$. The enthalpy ($\Delta H^*$) and entropy ($\Delta S^*$) of activation for the electropolymerization reaction can be calculated from the k values.

The enthalpy (ΔH^*) and entropy (ΔS^*) of activation associated with k were calculated using the Eyring equation and are represented in Table 3:

$$k = \frac{RT}{Nh} e^{(\Delta S^*/R)} e^{(-\Delta H^*/RT)}, \tag{12}$$

where k is the rate constant, R is the universal gas constant, N is Avogadro's number, and h is Plank's constant. The values of ΔH^*, ΔS^*, and E_a were found to be 51.75, -43.44, and $54.18 \, \text{kJmol}^{-1}$, respectively.

By plotting (log (k/T vs. $1/T$) (Figure 6(c)), a linear relationship with a slope of $\Delta H^*/2.303$ and intercept of (log (R/Nh) + $\Delta S^*/2.303$ R) was obtained. From the slope and intercept, the values of (ΔH^*) and (ΔS^*) are found to be $51.75 \, \text{kJmol}^{-1}$ and $-43.44 \, \text{JK}^{-1} \cdot \text{mol}^{-1}$, respectively. From the calculated (E_a, ΔH^* and ΔS^*), the formation of the activated complex step was endothermic, as indicated by the positive value of (ΔH^*).

3.2. Characterization of Poly(Salicylic Acid)

3.2.1. Electropolymerization Mechanism. The anodic oxidative polymerization of SA can be represented as follows::

3.2.2. Elemental Analysis. The elemental analysis data are represented in Table 3. The proposed structure of the obtained polymer is presented, and the data obtained from the elemental analysis were in a good agreement with the theoretical hypothesis of the proposed structure (see Scheme 1).

3.2.3. Ultraviolet-Visible Spectra. The UV spectra of the SA and PSA homopolymer are represented in Figure 7. The spectra showed the following absorption bands:

(1) For SA, three absorption bands were observed at $\lambda_{\max} = 230$, 270, and 277 nm, which may be attributed to the transition (E_2 band) of the benzene ring and β-band (A_{1g}-B_{2u}), respectively.

(2) For PSA, four absorption bands appeared at $\lambda_{\max} = 223$, 229, 232, and 265 nm, which may be due to the high conjugation of the aromatic polymeric chains.

3.2.4. Infrared Spectroscopy. The infrared spectra of SA and PSA are represented in Figure 8. The infrared absorption bands are also tabulated in Table 4.

3.2.5. ^{1}HNMR Spectroscopy. The ^{1}HNMR spectrum of PSA is represented in Figure 9; it shows two solvent signals at $\delta = 0.98$ ppm and $\delta = 2.50$ ppm. The protons of benzene rings in the polymeric structure were observed at $\delta = 6.29$ and $\delta = 6.90$ ppm. The singlet signal that appeared at $\delta = 9.50$ ppm was attributed to OH protons for the water solvation. The multiple signals at $\delta = 3.28$ ppm to $\delta = 3.43$ ppm are attributed to the OH proton of the carboxylic group.

3.2.6. Thermogravimetric Analysis. Thermogravimetric analysis (TGA) of PSA is represented in Figure 10. The TGA curve showed four stages.

In the first stage, including the removal of water in the temperature range from to $-100°C$, the weight loss was found to be 17.32% [47].
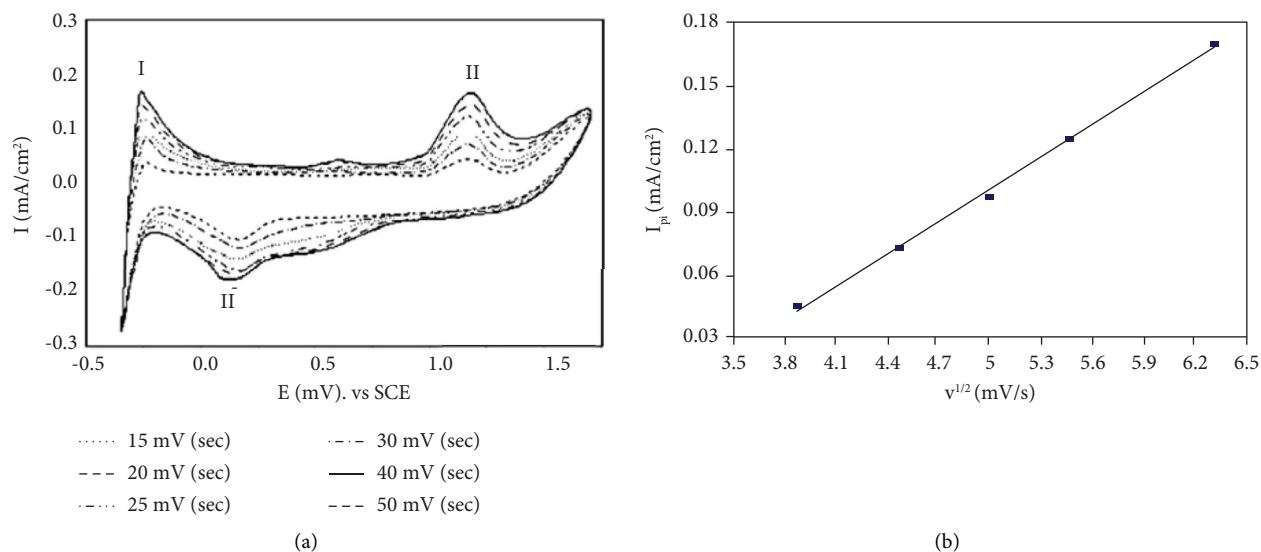
FIGURE 3: (a) Effect of the scan rate on the cyclic voltammograms for electropolymerization of SA from a solution containing $0.04\ \mathrm{mol\cdot L^{-1}}$ SA and $0.30\ \mathrm{mol\cdot L^{-1}}$ H_2SO_4 at 313 K. (b) Relationship between I_{pi} and $v^{1/2}$.

TABLE 2: Calculated values of the diffusion coefficient.

Scan rate (Vs^{-1})	Diffusion coefficient, (D) ($m^2 s^{-1}$)
0.015	1.85×10^{-7}
0.020	1.76×10^{-7}
0.025	1.62×10^{-7}
0.030	1.53×10^{-7}
0.040	1.34×10^{-7}

The next stage involved the loss of CO_2 molecules in the temperature range up to 130°C; the weight loss for this step was found to be 20.80%.

The third step was in the temperature range between 130 and –384°C, which included the loss of the benzene ring, and the weight loss was found to be (34.77%).

The last step was above 400°Cm, which involved the decomposition of the remaining part of the polymer, and the weight loss for this stage was found to be (27.11%).

3.2.7. Surface Morphology and X-Ray Diffraction.

The color of the PSA film deposited on the Pt electrode is gray, and it is homogeneous and adheres well to the surface of the electrode. The morphology of the PSA film was examined by SEM and XRD as well.

Figure 11(a) displays the SEM micrograph which shows a smooth lamellar surface. The XRD pattern indicated that PSA is a crystalline surface, as shown in Figure 11(b).

3.3. Application of PSA as a Corrosion Inhibitor for Mild Steel in 1 M H_2SO_4

3.3.1. Open Circuit Potential Measurements.

Figure 12 represents the open circuit potential of mild steel in the presence of different concentrations of PSA (blank, 20, 50, and 100 ppm), followed over 1 hour in a stagnant naturally aerated aqueous solution of 1 M H_2SO_4. The results showed that the presence of PSA shifted the steady-state potential to less negative values, Figure 12.

3.3.2. Potentiodynamic Polarization (The Tafel Extrapolation) Technique.

The electrochemical behavior of mild steel was investigated at different concentrations of PSA (blank, 20, 50, and 100 ppm) in 1 M H_2SO_4; the linear polarization and Tafel extrapolation techniques were used at a scan rate of $10\ \mathrm{mVs^{-1}}$. Figure 13 illustrates the potentiodynamic polarization curves after holding the mild steel electrode at the open circuit potential for 1 hr. It was evident that the corrosion potential shifted to the negative direction in the presence of different concentrations of PSA and both the anodic and cathodic current density decreased, indicating that PSA acts as a mixed inhibitor. The inhibition efficiency of the inhibitor may be attributed to its structure, as the inhibition efficiency will increase with increasing the chain length, resulting in an increase in the covered metal surface area as well as the electronic structure of both the inhibitor and the metal [51, 52].

The values of the corrosion parameters, (Tafel slopes (β_a and β_b) corrosion potential E_{corr}, corrosion current density i_{corr}, corrosion rate, and the corrosion protection efficiency ($\eta\%$)) [53], of the polymer coat film were calculated and are represented in Table 5.

Table 5: shows that the Tafel slopes (β_a and β_b) decreased in most cases with increasing PSA concentration, indicating that the corrosion process was under activation control. The corrosion current density (i_{corr}) was measured after immersion of a mild steel electrode for 1 hr in 1 M H_2SO_4; the corrosion rate decreased with increasing PSA concentration, indicating that PSA has better corrosion resistance.

3.3.3. The Electrochemical Impedance Measurements.

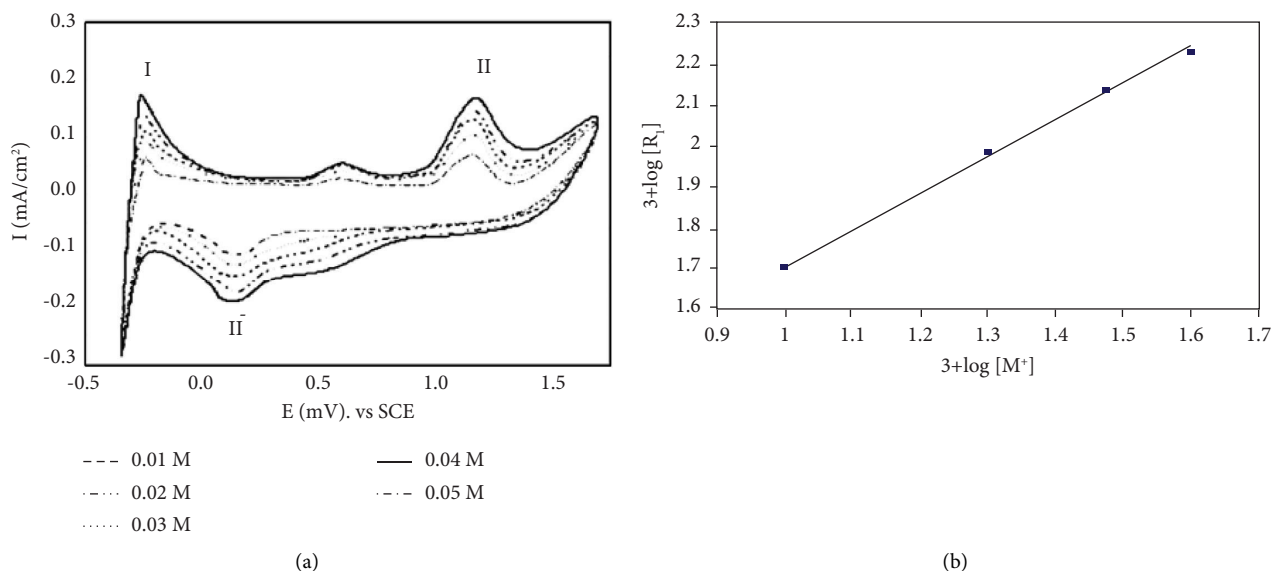Impedance measurement of PSA is illustrated in Figure 14 in the form of Nyquist plots (Figure 14(a)) and Bode plots

(a)

(b)

FIGURE 4: (a) Effect of SA concentration on the cyclic voltammograms for the electropolymerization reaction from a solution containing 0.30 mol·L^{-1} H$_2$SO$_4$ at 313 K with a scan rate 40 mVs^{-1}. (b) Double logarithmic plot of the initial rate for the electropolymerization reaction versus different SA concentrations.

(a)

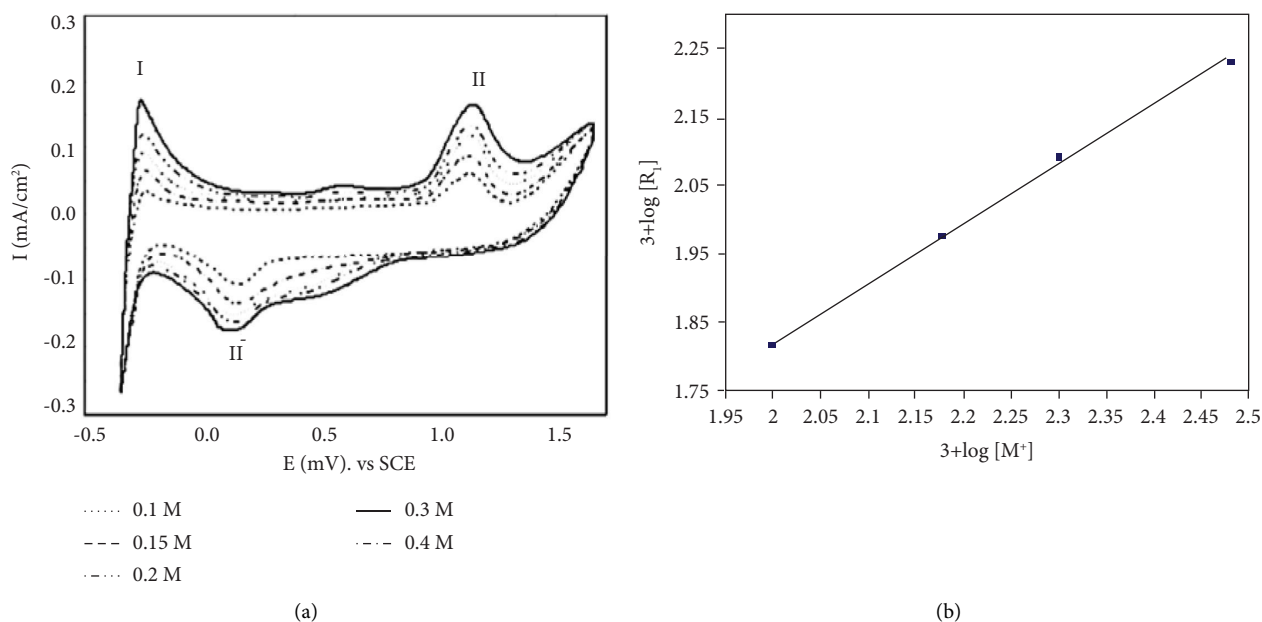(b)

FIGURE 5: (a) Effect of H$_2$SO$_4$ concentration on the cyclic voltammograms for electropolymerization of 0.04 mol·L^{-1} SA at 313 K with a scan rate of 40 mVs^{-1}. (b) Double logarithmic plot of the initial rate for the electropolymerization reaction versus different H$_2$SO$_4$ concentration values.

(Figure 14(b)). The system response of the complex plane in the Nyquist plot consists of a semicircle. The time constant or diameter of the semicircle increases with increasing polymer concentration. Figure 14(b) shows that there is a maximum of one phase for the mild steel electrode with intermediate frequency. This one-time constant appeared as a well-defined capacitive loop in the intermediate frequency region of the Nyquist presentation. The intermediate time constant was due to the presence of a protective film on the surface [39, 40].

The data can be adjusted utilizing the simple Randles model (Figure 15), which consists of a parallel combination between C_{dl}, double layer capacitance, Rct, charge transfer resistance, all in series with R_s, solution resistance, and R_p is polarization resistance. The data are fitted and represented in Table 6, which shows that the equivalent circuit parameter of
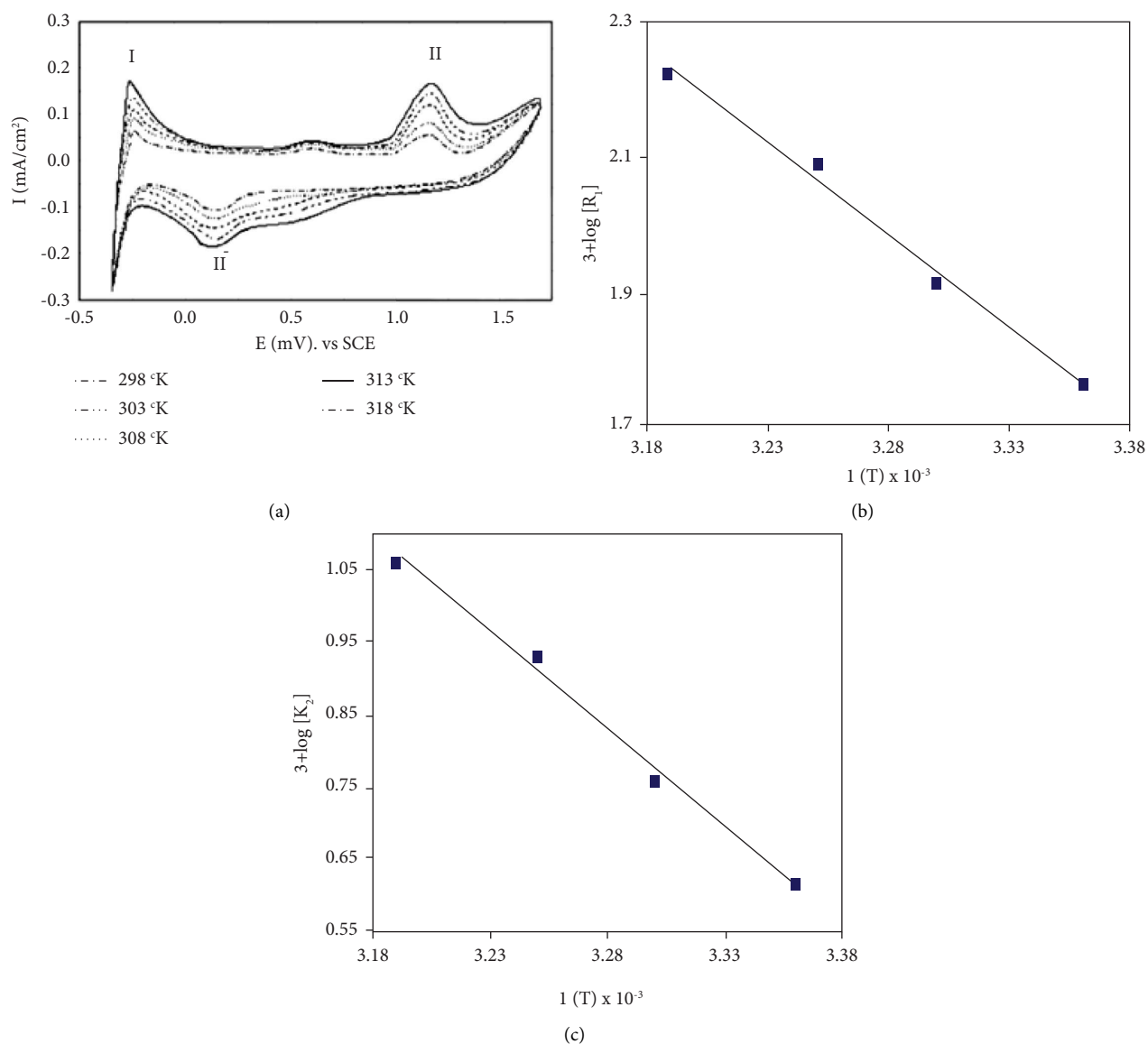
(a)

(b)

(c)

FIGURE 6: (a) Effect of temperature on the cyclic voltammograms. (b) Arrhenius plot. (c) Eyring plot of the anodic oxidative electro-polymerization of SA from a solution containing $0.04\,\mathrm{mol\cdot L^{-1}}$ SA and $0.30\,\mathrm{mol\cdot L^{-1}}$ H_2SO_4, with a scan rate of $40\,\mathrm{mVsec^{-1}}$.

TABLE 3: Elemental analytical data of the prepared polymer.

Polymer name	*C*		*H*		*O*		*S*	
	Cal.	Found	Cal.	Found	Cal.	Found	Cal.	Found
PSA	51.66	49.87	3.08	3.42	41.32	41.35	3.94	5.36

a mild steel electrode after immersion for 1 hr in naturally aerated 1 M H_2SO_4 in the presence of PSA at 25°C, and also C_{dl} (the adsorbed layer thickness $1/C_{dl}$) decreased with increasing polymer concentration. The calculated equivalent circuit parameters indicated that PSA formed a passive protective layer on the steel surface.
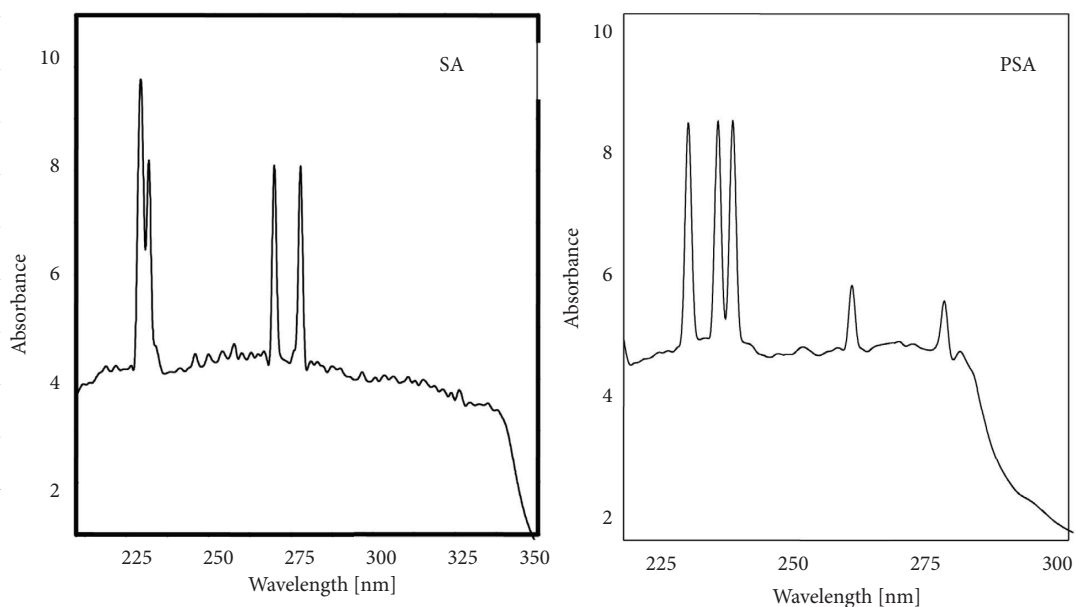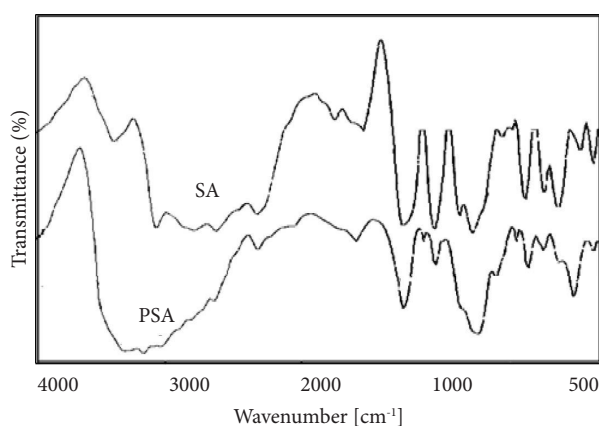
Figure 7: UV assignments of SA and PSA.

Figure 8: The infrared spectra of SA and PSA.

Table 4: Infrared absorption bands of SA and PSA.

| Assignments	Wavenumber (cm^{-1})	
	SA	PSA
CH out-of-plane bending for 1, 2 di-substituted benzene ring.	580^s	680^s
	768^w	763^m
CH out-of-plane bending for 1, 2, and 4 tri-substituted benzene ring.	869^m	886^s
Stretching vibration for C-O group.	—	1024^w
Stretching for incorporation in the polymer sulfate group.	1218^b	1193^b
Stretching vibration of C=C in benzene ring	1456^s	1454^m
	1656^b	1660^s
	2600^w	2597^b
	2876^w	2856^s
Stretching vibration for CH aromatic	—	2999^w
	—	3233^b
Stretching vibration intermolecular hydrogen of solvated OH group or end group OH of polymeric chain.	3496^b	3437^w

(where s: strong, w: weak, b: broad, and m: medium).
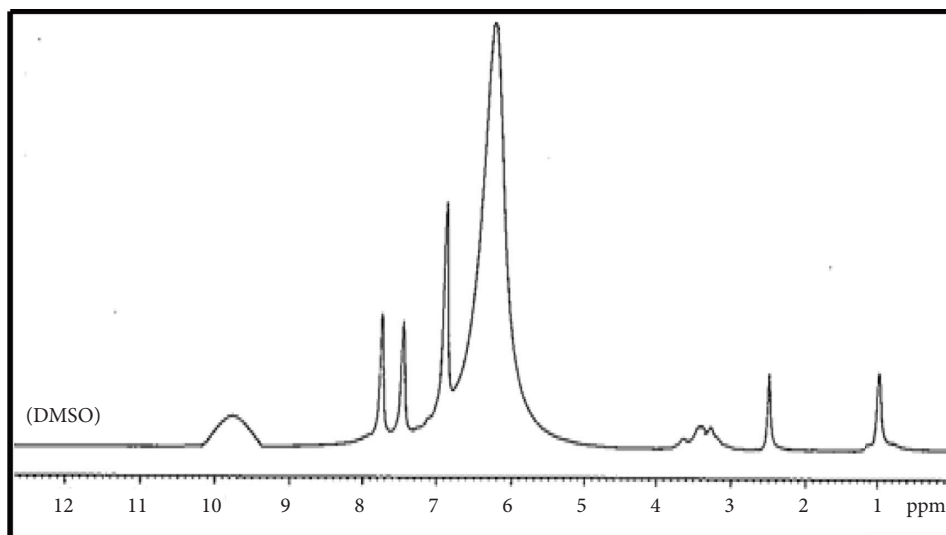
FIGURE 9: ^{1}HNMR spectra of PSA.
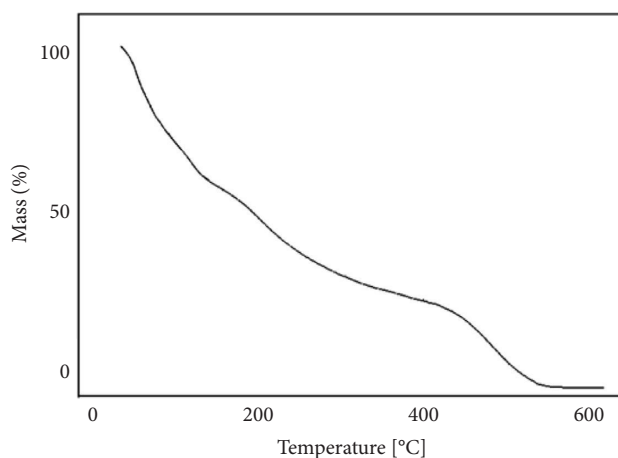
FIGURE 10: Thermogravimetric analysis (TGA) of PSA.

3.3.4. Mechanism of Inhibition Action

(1) Adsorption Isotherm. The data represented in Figure 16 showed that the adsorption process in accordance with the Langmuir adsorption isotherm.

$$K_{\text{ads}}{}^* C = \frac{\theta}{(1 - C)}, \tag{13}$$

where (K_{ads}) is the equilibrium constant of the adsorption process, (C) is the molar concentration of inhibitors by molarity, and (θ) is surface coverage value for the prepared inhibitor. The results indicated that the prepared inhibitor was highly adsorbed on the surface of mild steel forming a protective film. The calculated (K_{ads}) values were used to determine the standard free energy, $\Delta G^{\text{o}}{}_{\text{ads}}$ as follows:

$$\Delta G^o_{\text{ads}} = \left(\frac{1}{55.5}\right) e^{\left(- K_{\text{ads}}/RT\right)}, \tag{14}$$

where (55.5) is the value of the water concentration in solution and R is the gas constant at standard conditions.

From the data values, it was found that the value of ΔG_{ads} was -9.7 kJ/mol proved that the adsorption process was a spontaneous physisorption process. This revealed that the inhibition process occurred via an electrostatic interaction between the charged inhibitor molecules and the (physically) charged metal surface.

(2) Quantum Calculations. Experimental measurements revealed that the corrosion inhibition of the synthesized PSA polymer increased with concentration and reached 74% for 100 ppm. It was reported that polymers have attracted attention due to the presence of delocalization of π-electrons, so at lower concentrations they could serve as efficient corrosion inhibitors if compared with the simple molecules [7, 55]. Thus, one may conclude that the inhibition efficiency of PSA is higher than that of SA, which has a 47% inhibition efficiency [36]. To modulate the adsorption of PSA on the metal surface, some molecular and electronic properties along with the adsorption energies of the basic SA monomer and its dimers were determined using DFT calculations and
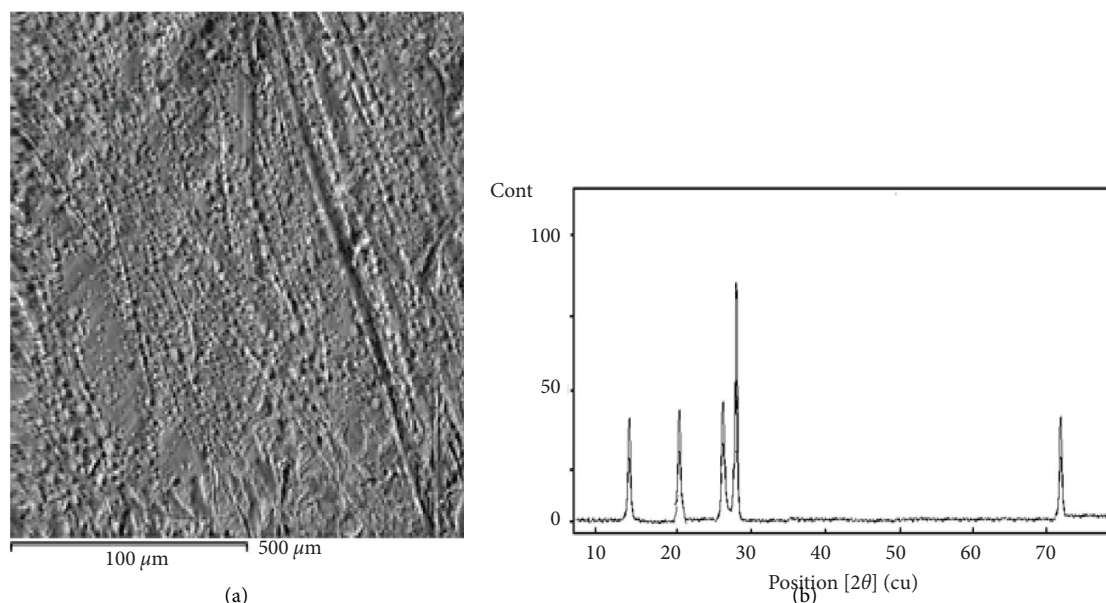
Figure 11: (a) Scanning electron microscope (SEM) and (b) X-ray diffraction (XRD) of PSA.
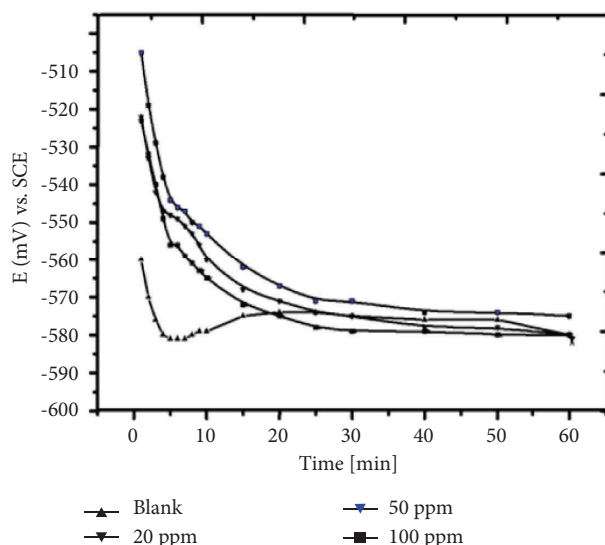

Figure 12: Variation of the open-circuit potential of mild steel with time in a stagnant naturally aerated aqueous solution of 1 M H_2SO_4 at different concentrations of PSA at 25°C.

molecular mechanics, as mentioned in Materials and Methods. The molecular and electronic properties of SA and its dimer calculated in a water solvent are presented in Table 7.

The calculated properties indicated the higher reactivity of the dimer compared with its monomer. For instance, the energy gap of the dimer showed a variation of 0.1 eV compared to the monomer. The calculated (ΔN) indicated the transfer of electrons from the inhibitor to the interface of metal/solution (ΔN). This indicated that these compounds may tend to give electrons to the interface of metal/solution. The optimized geometries, ESP, and frontier molecular orbitals of the monomer and its dimer are represented in

Figure 17. The red and blue regions on the ESP indicated that the donor/acceptor atomic sites of SA and its dimer. HOMO and LUMO orbitals showed more delocalization in the dimer compared with the monomer, which may also explain the higher inhibition efficiency of PSA.

Figure 18 shows the adsorption of SA and PSA on the mild steel surface. The calculated adsorption energies of SA and PSA on the metal surface are −67.93 and −96.69 kcal·mol^{-1}. The more negative adsorption energy, the higher is the corrosion inhibition. The PSA showed higher adsorption energy on the surface compared with the SA, which may confirm the effective inhibition efficiency of the PSA.
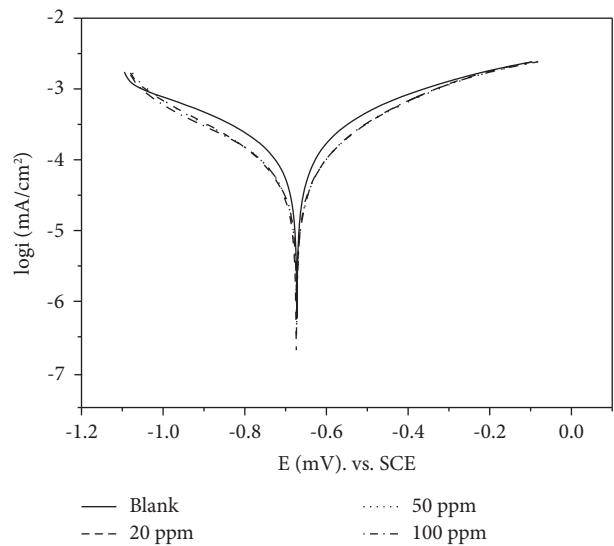
Figure 13: Potentiodynamic polarization curves of mild steel in a stagnant naturally aerated aqueous solution of 1 M H$_2$SO$_4$ at different concentrations of PSA at 25°C.

Table 5: Potentiodynamic polarization parameter of steel after 1 hr. of electrode immersion in a stagnant naturally aerated solution of 1 M H$_2$SO$_4$ at 25°C. containing different concentrations of PSA.

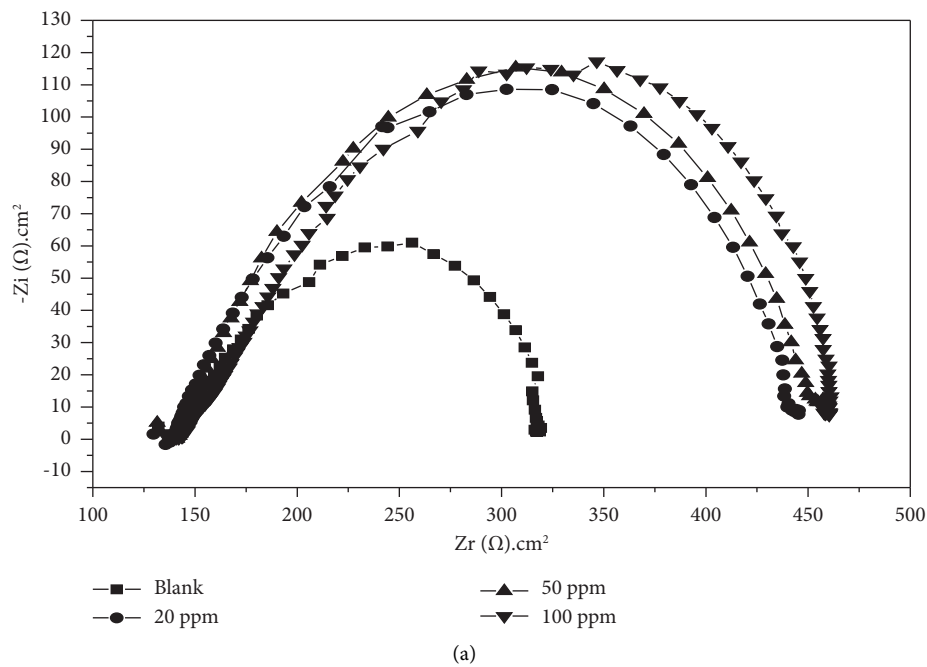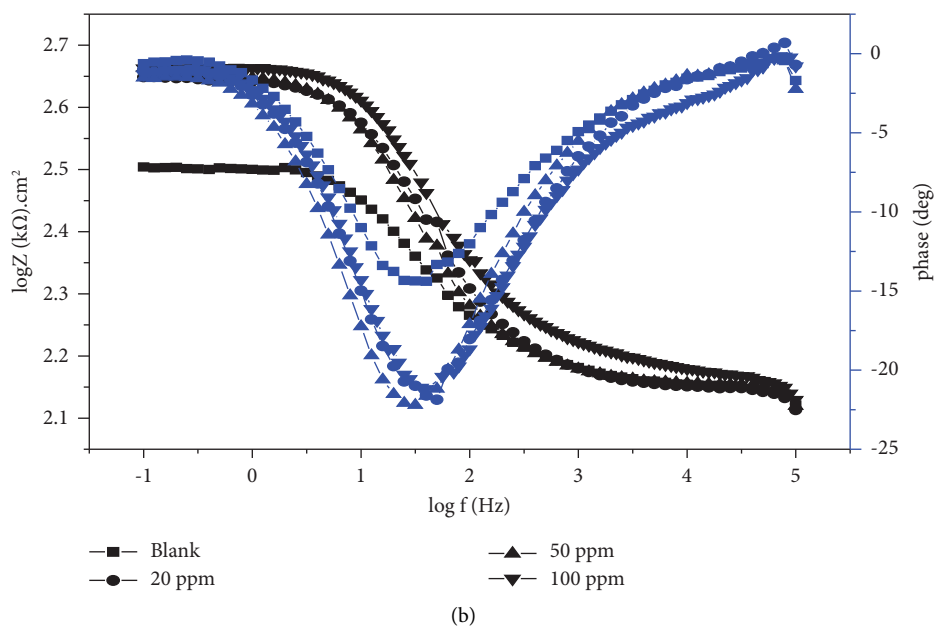| Concentration	E_{corr}/mV	R_p (kΩ.cm^2)	i_{corr} (μAcm^{-2})	β_a (mV/dec)	β_c (mV/dec)	Corrosion rate/μmy^{-1}	η (%)
Blank	−670.6	0.502	107.1	263.4	−345.1	1.330	0.00
20 ppm	−671.0	0.861	71.6	257.8	−364.1	0.890	33.2
50 ppm	−672.3	0.850	45.1	188.1	−244.6	0.562	57.9
100 ppm	−672.6	1.070	27.6	157.7	−180.9	0.343	74.2

(a)

Figure 14: Continued.

FIGURE 14: (a) Nyquist plot. (b) Bode plot of mild steel in a stagnant naturally aerated solution of 1 M H_2SO_4 at different concentrations of PSA at 25°C.
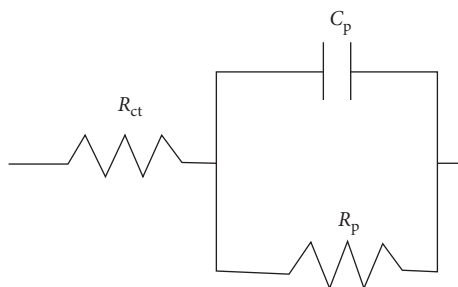

FIGURE 15: Equivalent circuit model for a simple electrochemical cell (Randles model).

TABLE 6: Equivalent circuit parameters for a mild steel electrode after immersion for 1 hr in a stagnant naturally aerated solution of 1 M H_2SO_4 at different concentrations of PSA at 25 C.

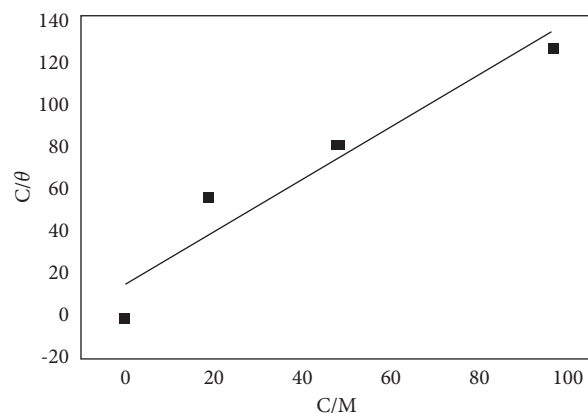| PSA concentration	$R_s / \Omega.cm^2$	R_p ($k\Omega cm^2$)	$C_{dl}/\mu Fcm^{-2}$
Blank	143.1	0.183	34.8
20 ppm	142.1	0.308	25.8
50 ppm	144.4	0.313	32.1
100 ppm	152.0	0.326	19.5

FIGURE 16: Langmuir isotherm plot for the adsorption of PSA on a mild steel surface in a stagnant, naturally aerated solution of 1 M H_2SO_4 at 25°C.

TABLE 7: Electronic and molecular properties of SA and PSA calculated in PCM model at the B3LYP/6-31G (d) level of theory.

	SA	PSA
Ionization potential, IP (eV)	6.34	6.44
Electron affinities, EA (eV)	1.50	1.70
Gap energy (eV)	4.84	4.74
χ (eV)	3.92	4.07
η (eV)	2.42	2.37
S (eV)	0.21	0.21
ω (eV)	3.18	3.50
ΔN	0.64	0.62
DM (Debye)	2.80	7.68
Corrosion inhibition efficiency	47%	74%

Optimized structure

ESP

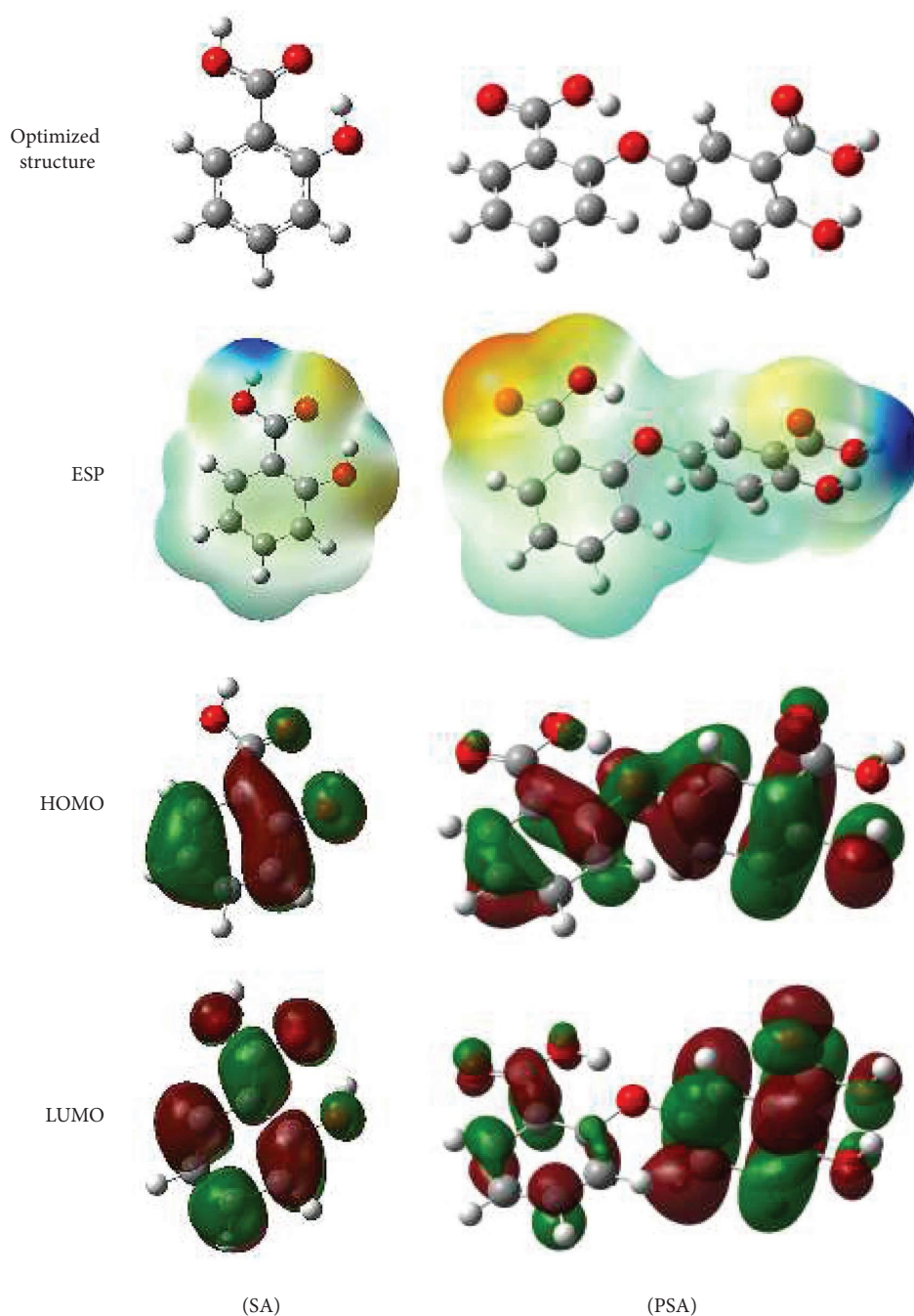HOMO

LUMO

(SA)   (PSA)

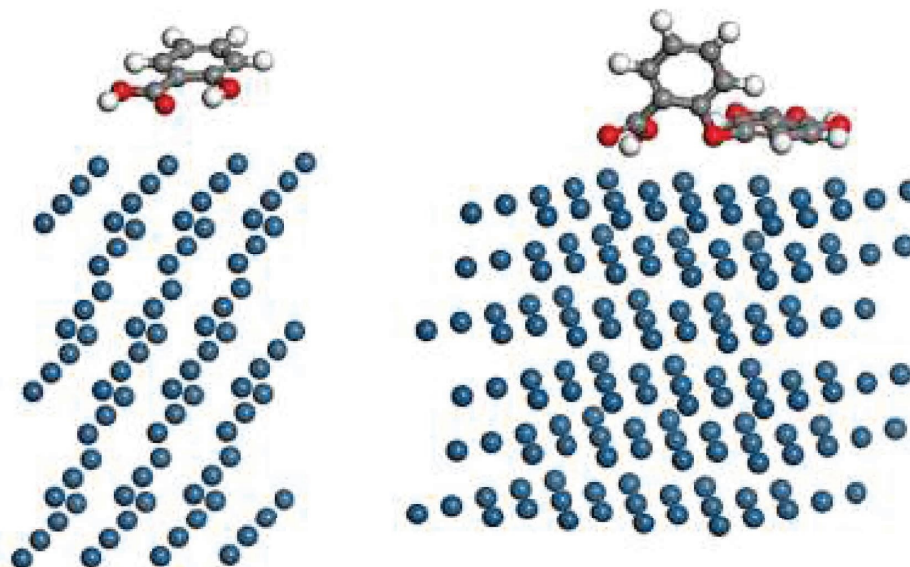FIGURE 17: Optimized geometries, ESPs, and frontier molecular orbitals of SA and PSA.

FIGURE 18: Adsorption of the monomer SA and PSA on the mild steel surface.

4. Conclusion

PSA was electropolymerized and deposited onto a Pt electrode. The kinetics measurements indicated that the polymer yield increased with increasing of the SA concentration, and H_2SO_4 concentration as well as the polymerization reaction temperature from 298 to –313 K proceeds.

The characterization of the deposited PSA indicated that it is thermally stable up to 400°C as shown in TGA data. The SEM micrographs and XRD patterns of the deposited PSA coatings showed that it has a smooth lamellar crystalline surface. A suggested polymerization mechanism was also proposed.

The potentiodynamic polarization and EIS measurements revealed that PSA may work as a mixed-type inhibitor, and the inhibition efficiency of 100 ppm of SA and PSA were found to be 48 and 74%, respectively. The adsorption isotherm revealed that the inhibition effect of PSA proceeds via a physisorption process, and the quantum calculations of the adsorption energy confirmed the effective inhibition behavior of the PSA.

Data Availability

The data used to support the findings of this study cannot be shared and are available upon reasonable request.

Conflicts of Interest

The authors declare that they have no conflicts of interest.

Acknowledgments

References

[1] H. M. Abd El-Lateef and A. O. Alnajjar, "Enhanced the protection capacity of poly (o-toluidine) by synergism with zinc or lanthanum additives at C-steel/HCl interface: a combined DFT, molecular dynamic simulations and experimental methods," *Journal of Molecular Liquids*, vol. 303, Article ID 112641, 2020.

[2] R. Karthikaiselvi and S. Subhashini, "The water soluble composite poly (vinylpyrrolidone–methylaniline): a new class of corrosion inhibitors of mild steel in hydrochloric acid media," *Arabian Journal of Chemistry*, vol. 10, pp. S627–S635, 2017.

[3] F. Ivušić, O. Lahodny-Šarc, H. O. Ćurković, and V. Alar, "Synergistic inhibition of carbon steel corrosion in seawater by cerium chloride and sodium gluconate," *Corrosion Science*, vol. 98, pp. 88–97, 2015.

[4] M. M. Solomon and S. A. Umoren, "Electrochemical and gravimetric measurements of inhibition of aluminum corrosion by poly (methacrylic acid) in H2SO4 solution and synergistic effect of iodide ions," *Measurement*, vol. 76, pp. 104–116, 2015.

[5] M. Hegazy, "Novel cationic surfactant based on triazole as a corrosion inhibitor for carbon steel in phosphoric acid produced by dihydrate wet process," *Journal of Molecular Liquids*, vol. 208, pp. 227–236, 2015.

[6] V. Srivastava and M. M. Singh, "Corrosion inhibition of mild steel in acidic medium by poly (aniline-co-o-toluidine) doped with p-toluene sulphonic acid," *Journal of Applied Electrochemistry*, vol. 40, no. 12, pp. 2135–2143, 2010.

[7] C. Jeyaprabha, S. Sathiyanarayanan, K. Phani, and G. Venkatachari, "Influence of poly (aminoquinone) on corrosion inhibition of iron in acid media," *Applied Surface Science*, vol. 252, no. 4, pp. 966–975, 2005.

[8] C. Jeyaprabha, S. Sathiyanarayanan, K. Phani, and G. Venkatachari, "Investigation of the inhibitive effect of poly (diphenylamine) on corrosion of iron in 0.5 M H_2SO_4 solutions," *Journal of Electroanalytical Chemistry*, vol. 585, no. 2, pp. 250–255, 2005.

[9] R. Karthikaiselvi and S. Subhashini, "Study of adsorption properties and inhibition of mild steel corrosion in hydrochloric acid media by water soluble composite poly (vinyl alcohol-o-methoxy aniline)," *Journal of the Association of Arab Universities for Basic and Applied Sciences*, vol. 16, no. 1, pp. 74–82, 2014.

[10] S. Sathiyanarayanan, K. Balakrishnan, S. Dhawan, and D. Trivedi, "Prevention of corrosion of iron in acidic media using poly (o-methoxy-aniline)," *Electrochimica Acta*, vol. 39, no. 6, pp. 831–837, 1994.

[11] S. Sathiyanarayanan, S. Dhawan, D. Trivedi, and K. Balakrishnan, "Soluble conducting poly ethoxy aniline as an inhibitor for iron in HCl," *Corrosion Science*, vol. 33, no. 12, pp. 1831–1841, 1992.

[12] A. Madhankumar and N. Rajendran, "Poly (m-phenylendiamine-co-o-aminophenol) coatings on mild steel: effect of comonomers feed ratio on surface and corrosion protection aspects," *Progress in Organic Coatings*, vol. 76, no. 10, pp. 1445–1453, 2013.

[13] P. Muthirulan, N. J. S. Rajendran, and C. Technology, "Poly (o-phenylenediamine) coatings on mild steel: electrosynthesis, characterization and its corrosion protection ability in acid medium," *Surface and Coatings Technology*, vol. 206, no. 8-9, pp. 2072–2078, 2012.

[14] G. Ćirić-Marjanović, "Recent advances in polyaniline research: polymerization mechanisms, structural aspects, properties and applications," *Synthetic Metals*, vol. 177, pp. 1–47, 2013.

[15] M. Düdükcü, Y. A. Udum, Y. Ergün, and F. Köleli, "Electrodeposition of poly (4-methyl carbazole-3-carboxylic acid) on steel surfaces and corrosion protection of steel," *Journal of Applied Polymer Science*, vol. 111, no. 3, pp. 1496–1500, 2009.

[16] D. E. Tallman, G. Spinks, A. Dominis, and G. G. Wallace, "Electroactive conducting polymers for corrosion control," *Journal of Solid State Electrochemistry*, vol. 6, no. 2, pp. 73–84, 2002.

[17] G. M. Abd El-Hafeez, M. M. El-Rabeie, A. F. Gaber, and Z. R. Farag, "Electropolymerized durable coatings deposited onto Pt-electrode as corrosion inhibitor for mild steel," *Journal of Adhesion Science and Technology*, vol. 36, no. 11, pp. 1227–1246, 2021.

[18] G. M. Abd El-Hafeez, M. M. El-Rabeie, A. F. Gaber, Z. R. Farag, and Research, "Tailored polymer coatings as corrosion inhibitor for mild steel in acid medium," *Journal of Coatings Technology and Research*, vol. 18, no. 2, pp. 581–590, 2021.

[19] Z. R. Farag, M. E. Moustapha, E. H. Anouar, and G. M. Abd El-Hafeez, "The inhibition tendencies of novel hydrazide derivatives on the corrosion behavior of mild steel in hydrochloric acid solution," *Journal of Materials Research and Technology*, vol. 16, pp. 1422–1434, 2022.

[20] D. Sunil, P. Kumari, P. Shetty, and S. A. Rao, "Indole hydrazide derivatives as potential corrosion inhibitors for mild steel in HCl acid medium: experimental study and theoretical calculations," *Transactions of the Indian Institute of Metals*, vol. 75, no. 1, pp. 11–25, 2022.

[21] M. Abdallah, B. H. Asghar, I. Zaafarany, and A. J. I. J. E. S. Fouda, "The inhibition of carbon steel corrosion in hydrochloric acid solution using some phenolic compounds," *International Journal of Electrochemical Science*, vol. 7, no. 1, pp. 282–304, 2012.

[22] D. Veys-Renaux, S. Reguer, L. Bellot-Gurlet, F. Mirambet, and E. Rocca, "Conversion of steel by polyphenolic model molecules: corrosion inhibition mechanism by rutin, esculin, esculetol," *Corrosion Science*, vol. 136, pp. 1–8, 2018.

[23] T. Tüken, G. Arslan, B. Yazıcı, and M. Erbil, "The corrosion protection of mild steel by polypyrrole/polyphenol multilayer coating," *Corrosion Science*, vol. 46, no. 11, pp. 2743–2754, 2004.

[24] N. A. Aljeaban, L. K. M. O. Goni, B. G. Alharbi et al., "Polymers decorated with functional motifs for mitigation of steel corrosion: an overview," *International Journal of Polymer Science*, vol. 2020, no. 2020, pp. 1–23, 2020.

[25] Z. Meriem, F. Hana, D. Souad et al., "Experimental and theoretical evaluation of the adsorption process of some polyphenols and their corrosion inhibitory properties on mild steel in acidic media," *Journal of Environmental Chemical Engineering*, vol. 9, no. 6, Article ID 106482, 2021.

[26] A. Salhi, H. Amhamdi, M. El Massaoudi et al., "Preventive behavior of phenol Schiff bases on mild steel corrosion in acidic medium part A: experimental and molecular modeling approach," *Chemical Data Collections*, vol. 39, Article ID 100864, 2022.

[27] J. V. Nardeli, C. S. Fugivara, M. Taryba, E. R. Pinto, M. Montemor, and A. V. Benedetti, "Tannin: a natural corrosion inhibitor for aluminum alloys," *Progress in Organic Coatings*, vol. 135, pp. 368–381, 2019.

[28] A. Belakhdar, H. Ferkous, S. Djellali et al., "Computational and experimental studies on the efficiency of Rosmarinus officinalis polyphenols as green corrosion inhibitors for XC48 steel in acidic medium," *Colloids and Surfaces A: Physicochemical and Engineering Aspects*, vol. 606, Article ID 125458, 2020.

[29] S. Aourabi, M. Driouch, M. Sfaira et al., "Phenolic fraction of Ammi visnaga extract as environmentally friendly antioxidant and corrosion inhibitor for mild steel in acidic medium," *Journal of Molecular Liquids*, vol. 323, Article ID 114950, 2021.

[30] I.-M. Chung, S.-H. Kim, and M. Prabakaran, "Evaluation of phytochemical, polyphenol composition and anti-corrosion capacity of Cucumis anguria L. leaf extract on metal surface in sulfuric acid medium," *Protection of Metals and Physical Chemistry of Surfaces*, vol. 56, no. 1, pp. 214–224, 2020.

[31] P. N. Moghaddam, R. Amini, P. Kardar, and B. Ramezanzadeh, "Synergistic corrosion inhibition effects of the non-hazardous cerium nitrate and tannic acid polyphenolic molecules on the surface of mild-steel in chloride-containing solution: detailed surface and electrochemical explorations," *Journal of Molecular Liquids*, vol. 322, Article ID 114510, 2021.

[32] J. D. Chelaru, M. Ciobra, M. Ciobra, and L. M. Muresan, "Inhibition effect of some commercial corrosion inhibitors on mild steel in 7.0 M phosphoric acid," *Studia Universitatis Babes-Bolyai, Chemia*, vol. 65, no. 1, pp. 17–26, 2020.

[33] S. Shahen, "Study of corrosion inhibition for mild steel in hydrochloric acid solution by new polyester derivative (glyptal)," *Al-Azhar Bulletin of Science*, vol. 30, no. 1, pp. 47–54, 2019.

[34] A. Alamiery, A. B. Mohamad, A. A. H. Kadhum, and M. S. Takriff, "Comparative data on corrosion protection of mild steel in HCl using two new thiazoles," *Data in Brief*, vol. 40, Article ID 107838, 2022.

[35] M. M. El-Naggar, A. S. Amin, S. M. Syam, S. M. Refaat, and B. N. Ahmed, "Inhibition mechanism of mild steel corrosion in acidic media by some amine compounds," *Benha Journal of Applied Sciences*, vol. 7, no. 4, pp. 231–237, 2022.

[36] S. Bilgiç, "The inhibition effects of benzoic acid and salicylic acid on the corrosion of steel in sulfuric acid medium," *Materials Chemistry and Physics*, vol. 76, no. 1, pp. 52–58, 2002.

[37] N. Hebbar, B. M. Praveen, B. M. Prasanna, T. V. Venkatesha, and S. B. Abd Hamid, "Anthranilic acid as corrosion inhibitor for mild steel in hydrochloric acid media," *Procedia Materials Science*, vol. 5, pp. 712–718, 2014.

[38] S. B. Ade, "Corrosion inhibition of mild steel in different acid medium by using various acidic groups of organic compounds," *International Journal for Research in Applied Science and Engineering Technology*, vol. 10, no. 2, pp. 367–373, 2022.

[39] J. Diggle, T. Downie, and C. Goulding, "The dissolution of porous oxide films on aluminium," *Electrochimica Acta*, vol. 15, no. 7, pp. 1079–1093, 1970.

[40] K. M. Ismail, A. A. El-Moneim, and W. A. Badawy, "Stability of sputter-deposited amorphous Mn-Ta alloys in chloride-free and chloride-containing $H_2 SO_4$ solutions," *Journal of the Electrochemical Society*, vol. 148, no. 2, pp. C81–C87, 2001.

[41] S. M. Sayyah, M. M. El-Rabiei, G. M. Abd El-Aafez, and A. F. Gaber, "Electropolymerization of ortho-bromophenol on Pt-electrode from aqueous acidic solution; kinetics, mechanism, electrochemical studies and characterization of the polymer obtained," *International Journal of Advanced Research*, vol. 3, no. 9, pp. 65–84, 2015.

[42] G. W. T. M. J. Frisch, H. B. Schlegel, G. E. Scuseria et al., "Gaussian 16 Rev. C.01," 2016, https://gaussian.com/man/.

[43] R. G. Pearson, "Hard and soft acids and bases," *Journal of the American Chemical Society*, vol. 85, no. 22, pp. 3533–3539, 1963.

[44] J. Tomasi, B. Mennucci, and R. Cammi, "Quantum mechanical continuum solvation models," *Chemical Reviews*, vol. 105, no. 8, pp. 2999–3094, 2005.

[45] G. Arslan, B. Yazici, and M. Erbil, "The effect of pH, temperature and concentration on electrooxidation of phenol," *Journal of Hazardous Materials*, vol. 124, no. 1-3, pp. 37–43, 2005.

[46] M. Gattrell and D. W. Kirk, "A study of electrode passivation during aqueous phenol electrolysis," *Journal of the Electrochemical Society*, vol. 140, no. 4, pp. 903–911, 1993.

[47] S. M. Sayyah, S. S. Abd El-Rehim, M. M. El-Deeb, S. M. Kamal, and R. E. Azooz, "Electropolymerization of p-phenylenediamine on Pt-electrode from aqueous acidic solution: kinetics, mechanism, electrochemical studies, and characterization of the polymer obtained," *Journal of Applied Polymer Science*, vol. 117, no. 2, pp. 943–952, 2010.

[48] U. Evans, *Introduction to Metallic Corrosion*, Edward Arnold, London, UK, 3rd edition, 1981.

[49] J. E. B. Randles, "A cathode ray polarograph. Part II.—the current-voltage curves," *Transactions of the Faraday Society*, vol. 44, no. 0, pp. 327–338, 1948.

[50] M. Ureta-Zanartu, P. Bustos, M. Diez, M. Mora, and C. Gutierrez, "Electro-oxidation of chlorophenols at a gold electrode," *Electrochimica Acta*, vol. 46, no. 16, pp. 2545–2551, 2001.

[51] N. Hajjaji, I. Rico, A. Srhiri, A. Lattes, M. Soufiaoui, and A. Ben Bachir, "Effect of N-alkylbetaines on the corrosion of iron in 1 M HCl solution," *Corrosion*, vol. 49, no. 4, pp. 326–334, 1993.

[52] A. Popova, E. Sokolova, and S. Raicheva, "Relationship between the molecular structure of organic inhibitors and their protective action. II. Inhibitors in acidic media," *Khim. Ind.*, vol. 60, no. 2, pp. 72–76, 1988.

[53] W. Badawy, F. Al-Kharafi, and A. El-Azab, "Electrochemical behaviour and corrosion inhibition of Al, Al-6061 and Al–Cu in neutral aqueous solutions," *Corrosion Science*, vol. 41, no. 4, pp. 709–727, 1999.

[54] B. B. Damaskin, O. A. Petrii, and V. V. Batrakov, *Adsorption of Organic Compounds on Electrodes*, Plenum, New York, NY, USA, 1971.

[55] A. Joshi and K. Srivastava, "Studies on inhibitive-film protection of a water-soluble polymer on mild, steel," *Corrosion Prevention and Control*, vol. 36, no. 5, pp. 138–141, 1989.